J. Fluid Mech. (1982), *vol.* 114, *pp.* 467–480
Printed in Great Britain

The influence of side walls on finite-amplitude convection in a layer heated from below

By H. FRICK

Kernforschungszentrum Karlsruhe, Institut für Reaktorbauelemente, Karlsruhe, West Germany

AND R. M. CLEVER

TRW Systems, 1 Space Park, Redondo Beach, California 90278

(Received 22 May 1980 and in revised form 23 February 1981)

Finite-amplitude convection rolls of an infinite-Prandtl-number fluid in a long channel heated from below are investigated. Because of the side walls, the convection rolls depend on all three spatial co-ordinates, although only two velocity components are of importance for a wide range of Rayleigh numbers and aspect ratios. Accurately converged solutions are presented for a range of aspect ratios between 0 (Bénard convection) to 100 (Hele Shaw convection) and for Rayleigh numbers up to about 50 times the critical linear stability value. The influence of rigid versus slip boundaries as well as the wavelength of the convection rolls on the heat transport is investigated in detail. Comparisons with existing results for the analogous problem of convection in a porous medium indicates that the similarity tends to disappear at Rayleigh numbers less than a few times the critical value. Whenever possible, the theoretical findings are compared with experimental results. In all cases close agreement is found.

1. Introduction

For a fluid layer heated from below and of infinite horizontal extent, research performed during the past few decades has led to a virtually complete understanding of both the mode of convection and the heat transport over a wide range of Rayleigh numbers. In the case of fluids with Prandtl numbers greater than about ten it is known that two-dimensional convection rolls are the only stable form of convection up to about ten times the critical Rayleigh number at the onset of convection, $R_c = 1708$ (Busse 1978). In the present paper we intend to extend this work to the case of convection in a confined region with heating from below.

The introduction of confining walls into the convection layer removes the horizontal isotropy and causes the rolls to align themselves with axes perpendicular to the longer side of the container. This was first shown theoretically by Davis (1967) and demonstrated subsequently by the exact calculations of Davies-Jones (1970), in the case of free boundaries, and Frick & Clever (1980), in the case of rigid boundaries. The experimental work of Ozoe, Sayama & Churchill (1974) has verified the alignment of convection rolls suggested by Davis for the onset of convection and demonstrated their presence for Rayleigh numbers well into the nonlinear region. As a consequence of the presence of side walls the fluid motion depends on all three spatial co-ordinates. The viscous drag of the walls tends to restrain motions near the wall and thus introduces a

variation of the flow field in the direction of the roll axis. This is reflected by an increase in the critical Rayleigh number for the onset of convection as the distance between side walls is decreased. Equivalently, at a fixed value of the Rayleigh number for finite-amplitude convection the heat transport decreases with decreasing side-wall spacing. There is experimental evidence, however, that the influence of aspect ratio on the heat transport at high Rayleigh number is less pronounced than for the critical Rayleigh number. This has been shown in the experiments of Arnold (1978), Edwards, Arnold & Wu (1979) and Wu & Edwards (1980) for various aspect ratios (height to width) ranging up to eight and Rayleigh numbers up to about ten times the critical value. In the present paper this problem is investigated numerically. By studying in detail the dependence of the Nusselt number on the Rayleigh number and on the aspect ratio results are obtained that cover a much wider range of the parameter space than is covered by the experimental investigations.

In the limit of large aspect ratio the side walls cause a major simplification of the convective motions. The dependence of the velocity field in the direction parallel to the roll axes becomes quadratic and the resulting motion is referred to as Hele Shaw convection. It has been generally assumed for Hele Shaw convection that the heat transfer increases relatively strongly with Rayleigh number. In fact, Elder (1967) shows a linear relationship, $Nu \sim R/R_c$, whereas for ordinary convection $Nu \sim R^{0.3}$ has been generally accepted. Extrapolation of these expressions to large values of R at fixed aspect ratio would indicate the anomalous result that the side walls cause an increase in heat transfer above a certain value of R. We shall explore this interesting question by providing heat-transfer results for a wide range of Rayleigh numbers and aspect ratios and investigate the range of parameters for which the Hele Shaw approximation applies.

In the general case of convection in a confined region the side walls create an additional component of velocity. Unlike the situation in ordinary two-dimensional convection rolls, a component of vertical vorticity is generated by the temperature gradient parallel to the axis of the rolls. For finite-amplitude convection at large Prandtl number this remains the only mechanism for generating vertical vorticity. At the onset of convection this effect is quite small for rigid horizontal boundaries (Frick & Clever 1980), and for all practical purposes can be neglected. We therefore expect the influence of vertical vorticity to be small for the present case and shall neglect it in the analysis.

It is known that two-dimensional convection rolls become unstable to three-dimensional disturbances at $R_2 = 22\,600$ for a layer of infinite horizontal extent. Here the cross-roll instability causes a transition to three-dimensional bimodal convection (Busse 1978). For high aspect ratios this instability will be suppressed at the onset of convection. The motion is purely two-dimensional owing to the geometry. The stability analysis of nonlinear convection in a Hele Shaw cell by Kvernvold (1979) shows that the region of stable convection is limited by the Eckhaus instability and the oscillatory instability. For an aspect ratio of order unity or lower, transition to bimodal convection must be expected at high Rayleigh numbers of the order of R_2.

The paper begins with the formulation of the basic equations and numerical method of solution in §2. In §3 the results of the calculations and comparisons with previous theoretical and experimental work are presented. In §4 some concluding remarks are given.

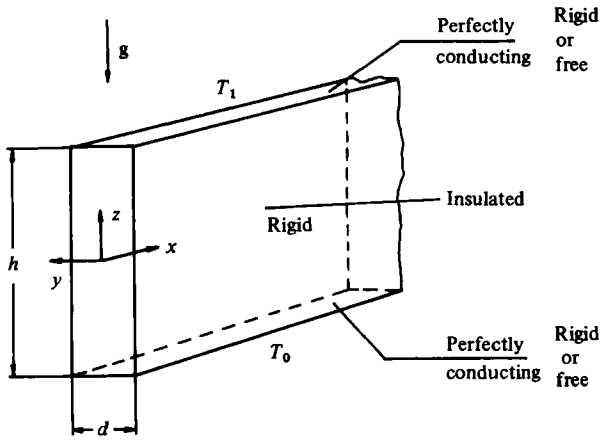

FIGURE 1. Geometry and co-ordinate system.

2. Mathematical formulation of the problem

We consider a fluid layer with spacing h of infinite horizontal extent in the x-direction and with side walls of spacing d in the y-direction as shown in figure 1. Constant temperatures T_1 and T_2 ($T_2 > T_1$) are prescribed at the upper and lower boundaries of the layer. For the non-dimensional description of the problem we use the thickness of the layer h as the length scale, h^2/κ, with κ denoting the thermal diffusivity, as the time scale, and $(T_2/T_1)/R$ as the temperature scale. Accordingly the Navier–Stokes equations for the velocity vector $\mathbf{v}$ and the heat equation for the deviation of temperature from the conductive state θ are

$$\nabla . \mathbf{v} = 0, \tag{1}$$

$$\nabla^2 \mathbf{v} + \mathbf{k}\theta - \nabla\Gamma = \frac{1}{P}(\mathbf{v} . \nabla\mathbf{v} + \partial_t \mathbf{v}), \tag{2}$$

$$\nabla^2\theta + R\mathbf{k} . \mathbf{v} = \mathbf{v} . \nabla\theta + \partial_t \theta. \tag{3}$$

Here and subsequently, the unit vectors $\mathbf{i}$, $\mathbf{j}$ and $\mathbf{k}$ denote the x, y and z (vertical) directions, respectively. The Laplacian

$$\nabla^2 = \partial^2_{xx} + A^2\partial^2_{yy} + \partial^2_{zz} \tag{4}$$

reflects the dependence of the problem on the non-dimensional ratio A of the height to width. The dependence of the problem has thus been reduced to the three dimensionless parameters

$$R = \frac{\gamma g \Delta T h^3}{\nu\kappa}, \quad P = \frac{\nu}{\kappa}, \quad A = \frac{h}{d},$$

where γ is the coefficient of thermal expansion, ν is the kinematic viscosity and g is the acceleration due to gravity. All terms that can be expressed as gradients in (2) are included in $\nabla\Gamma$. It is convenient to eliminate the equation of continuity (1) from the problem by introducing the following general representation for the solenoidal velocity field:

$$\mathbf{v} = \boldsymbol{\delta}\phi + \boldsymbol{\epsilon}\psi, \tag{5}$$

where the operators $\boldsymbol{\delta}$ and $\boldsymbol{\epsilon}$ are defined by

$$\boldsymbol{\delta}\phi = \nabla\mathbf{x}(\nabla\mathbf{x}\mathbf{j}\phi), \tag{6a}$$

$$\boldsymbol{\epsilon}\psi = \nabla\mathbf{x}(\mathbf{j}\psi). \tag{6b}$$

It is worthwhile to note that the unit vector $\mathbf{j}$ of the y-direction has been used in the representation (6) instead of the more commonly used $\mathbf{k}$ of the z-direction, because the side walls represent the most important boundary. The use of $\mathbf{k}$ would not allow a simple boundary-condition description for the case of convection rolls with side walls; as it does in the case of a layer of infinite horizontal extent investigated by Clever & Busse (1974).

After operating with $\mathbf{j}.\nabla\mathbf{x}(\nabla\mathbf{x})$ and $\mathbf{j}.\nabla\mathbf{x}$ on (2) we obtain the following equations for the scalar variables ϕ, ψ and θ:

$$\nabla^4\Delta_2\phi + A\partial^2_{yz}\theta = (1/P)\{\boldsymbol{\delta}.((\boldsymbol{\delta}\phi+\boldsymbol{\epsilon}\psi).\nabla(\boldsymbol{\delta}\phi+\boldsymbol{\epsilon}\psi)) + \partial_t\nabla^2\Delta_2\phi\}, \tag{7a}$$

$$\nabla^2\Delta_2\psi + \partial_x\theta = (1/P)\{\boldsymbol{\epsilon}.((\boldsymbol{\delta}\phi+\boldsymbol{\epsilon}\psi).\nabla(\boldsymbol{\delta}\phi+\boldsymbol{\epsilon}\psi)) + \partial_t\Delta_2\psi\}, \tag{7b}$$

$$\nabla^2\theta + R(A\partial^2_{yz}\phi + \partial_x\psi) = (A\partial^2_{xy}\phi - \partial_z\psi)\,\partial_x\theta - A\Delta_2\phi\partial_y\theta + (A\partial^2_{yz}\phi + \partial_x\psi)\,\partial_z\theta + \partial_t\theta, \tag{7c}$$

where Δ_2 denotes the Laplacian with respect to the (x, z)-plane:

$$\Delta_2 = \partial^2_{xx} + \partial^2_{zz}. \tag{8}$$

Equations (7*a–c*) represent a set of coupled nonlinear partial differential equations in the scalar variables ϕ, ψ and θ. In addition to the coupling of the variables ϕ and ψ through the differential equations, in the case of rigid upper and lower surfaces this coupling occurs in the boundary conditions as well, as long as both ϕ and ψ are present (see Frick & Clever 1980). As has been shown by Davies-Jones (1970) in the case of free boundaries for the linear stability problem, solutions of the equations which contain components of both ϕ and ψ represent a more general solution for which the critical Rayleigh number for the onset of convection must be lower than for solutions in which ϕ is absent. In the case of free upper and lower boundaries the differences in the critical Rayleigh numbers between solutions with and without ϕ are most a few per cent. In the case of rigid boundaries the difference is substantially lower; at most about 1 % at aspect ratio 0·5, with the difference falling rapidly with either a smaller or larger value of A (Frick & Clever 1980). Hence we may conclude that the role of ϕ in the representation of the velocity field is of minor significance for this *linear* problem. However, in the case of nonlinear convection, the nonlinearity of the equations of motion introduces an additional coupling between ϕ and ψ. This is caused by the fact that the term

$$(1/P)\boldsymbol{\delta}.[(\boldsymbol{\epsilon}\psi.\nabla)\boldsymbol{\epsilon}\psi]$$

in (7*a*) is non-zero for scalar fields ψ which depend on y. Since we are not able to assess *a priori* the influence of ϕ on the ψ-component of the velocity caused by the nonlinear coupling, we solve the problem only in the case of a large-Prandtl-number fluid, where this coupling no longer exists. We also rely on the established linear-stability results which have demonstrated that the neglect of $\partial^2_{yz}\theta$ affects the results only

slightly. Hence we shall solve the equations under the assumption $\partial_{yz}^2\theta = 0$ and $\phi = 0$. We shall leave the problem of a finite-Prandtl-number fluid to a later time.

In the limit of large Prandtl numbers we approximate (7*a–c*) by a simpler set of equations in which ϕ is absent. In this approximation the generation of a scalar field ϕ by the perturbation temperature field of the linear term $\partial_{yz}\theta$ is neglected, and in the case of steady convection rolls the following equations result:

$$\nabla^2\Delta_2\psi + \partial_x\theta = 0, \tag{9}$$

$$\nabla^2\theta + R\partial_x\psi = -\partial_z\psi\partial_x\theta + \partial_x\psi\partial_z\theta. \tag{10}$$

We note that the scalar fields ψ and θ depend on all three spatial co-ordinates. The boundary conditions at the horizontal boundaries of the layer are given by

$$\psi = \partial_z\psi = \theta = 0, \quad \psi = \partial_{zz}^2\psi = \theta = 0 \quad (z = \pm\tfrac{1}{2}) \tag{11a, b}$$

for rigid and free surfaces respectively. Here it is assumed that the thermal conductivity of the solid region far exceeds that of the fluid. At the vertical bounding surfaces the boundary conditions are given by

$$\psi = \partial_y\theta = 0 \quad (y = \pm\tfrac{1}{2}), \tag{12}$$

where we have assumed rigid, adiabatic surfaces.

We solve (9) and (10) numerically, using the Galerkin method. Accordingly, we expand the variables ψ and θ in terms of a series sum of orthogonal functions:

$$\psi = \sum_{\lambda\nu\beta} ic_{\lambda\nu\beta} h_\nu^y(y)\, h_\beta^z(z)\, e^{i\lambda ax} \equiv \sum_{\lambda\nu\beta} ic_{\lambda\nu\beta}\psi_{\lambda\nu\beta}, \tag{13}$$

$$\theta = \sum_{\lambda\nu\beta} b_{\lambda\nu\beta} f_\nu^y(y) f_\beta^z(z)\, e^{i\lambda ax} \equiv \sum_{\lambda\nu\beta} b_{\lambda\nu\beta}\theta_{\lambda\nu\beta}. \tag{14}$$

Since the basic equations (9) and (10) contain an even number of y-derivatives, the solutions may be separated into non-combining sets, which are either even or odd in the y-direction. Since the critical Rayleigh number of the even-y solutions is lower than that of the odd solution, we may expand in the following sets of functions, which satisfy the boundary conditions:

$$h_\nu^y(y) = \cos[(2\nu - 1)\pi y], \tag{15}$$

$$f_\nu^y(y) = \cos[(2\nu - 2)\pi y]. \tag{16}$$

The functions

$$h_\beta^z(z) = \begin{Bmatrix} S_{\frac{1}{2}\beta}(z) & (\beta \text{ even}) \\ C_{\frac{1}{2}(\beta+1)}(z) & (\beta \text{ odd}) \end{Bmatrix}, \tag{17}$$

$$h_\beta^z(z) = \sin[\beta\pi(z + \tfrac{1}{2})] \tag{18}$$

satisfy the rigid- and free-surface boundary conditions for ψ, (11*a*) and (11*b*) respectively. Both (17) and (18) represent complete sets of alternating odd and even functions for alternating values of β. The use of (17) for convection problems was introduced by Chandrasekhar (1961, p. 635) for problems in which a scalar variable must satisfy four boundary conditions of the type (11*a*) for ψ.

The functions

$$f_\beta^z(z) = \sin[\beta\pi(z + \tfrac{1}{2})] \tag{19}$$

for θ are identical with the free-boundary representation (18) for ψ. The summation in expressions (13) and (14) runs through all integers $-\infty < \lambda < +\infty$ ($c_{0\nu\beta}$ excluded), $1 \leqslant \nu \leqslant \infty$ and $1 \leqslant \beta < \infty$. As in Clever & Busse (1974) the symmetry of (9) and (10) allows us to restrict ourselves to the case of a reduced subset of functions in the x-direction. With the present representation for ψ and θ we may restrict ourselves to solutions for which

$$c_{\lambda\nu\beta} = -c_{-\lambda\nu\beta}, \tag{20a}$$

$$b_{\lambda\nu\beta} = b_{-\lambda\nu\beta}, \tag{20b}$$

and it is convenient to introduce a trigonometric representation for the x-dependence of the problem instead of the complex representation $ic_{\lambda\nu\beta}$ used in (13). Hence we replace $e^{i\lambda\alpha x}$ in (13) and (14) by

$$h^x_\lambda(x) = \sin\lambda\alpha x, \tag{21a}$$

$$f^x_\lambda(x) = \cos\lambda\alpha x \tag{21b}$$

respectively. Accordingly, $ic_{\lambda\nu\beta}$ is replaced by $c_{\lambda\nu\beta}$ in (13).

For application of the Galerkin method we substitute expressions (13) and (14) into (9) and (10), multiply by $\psi_{\kappa\mu\gamma}$ and $\theta_{\kappa\mu\gamma}$ respectively, and average over the fluid region. The following set of coupled nonlinear algebraic equations for $c_{\lambda\nu\beta}$ and $b_{\lambda\nu\beta}$ is obtained:

$$I^{11}_{\kappa\mu\gamma\lambda\nu\beta} c_{\lambda\nu\beta} + I^{12}_{\kappa\mu\gamma\lambda\nu\beta} b_{\lambda\nu\beta} = 0, \tag{22a}$$

$$I^{21}_{\kappa\mu\gamma\lambda\nu\beta} b_{\lambda\nu\beta} + RI^{22}_{\kappa\mu\gamma\lambda\nu\beta} c_{\lambda\nu\beta} + I^{23}_{\kappa\mu\gamma\lambda\nu\beta\rho\pi\delta} c_{\lambda\nu\beta} b_{\rho\pi\delta} = 0, \tag{22b}$$

where the summation convention has been applied. For computational purposes it is necessary to restrict the unknown coefficients to a finite number. Following the methods developed by Busse (1967), Denny & Clever (1974) and subsequently Clever & Busse (1974) for the two-dimensional case, we introduce a trunction parameter N, such that all coefficients with

$$\lambda + \nu + \beta > N \tag{23}$$

are neglected. Hence the expressions in (22a) and (22b) extend over the range

$$\kappa + \mu + \gamma \leqslant N. \tag{24}$$

The calculation of the unknown coefficients $I^{nm}_{\kappa\mu\gamma\lambda\nu\beta}$ in (22) from the terms in (9) and (10) is straightforward. We denote an average over the fluid region by angular brackets, and write, for example

$$I^{11}_{\kappa\mu\gamma\lambda\nu\beta} = \langle \psi_{\kappa\mu\gamma} \nabla^4 \Delta_2 \psi_{\lambda\nu\beta} \rangle.$$

The set of equations (22) contains one further subset in which only variables with even values of $\lambda + \beta$ are present. Although this symmetry property does not exclude solutions in which both even and odd values of $\lambda + \beta$ are present, all solutions which exist close to the critical Rayleigh number are contained in this subset. Numerical experiments were performed in which attempts were made to generate solutions with both even and odd values of $\lambda + \beta$. In all cases, the coefficients with odd values of $\lambda + \beta$ approached zero as the solution converged. With the symmetry properties described above we solve (22a, b) for the coefficients $b_{\lambda\nu\beta}$ and $c_{\lambda\nu\beta}$ for various values of R, A and α. For values of $N = 9$, 11 and 13 we thus have 104, 195 and 328 unknown coefficients, which is a considerably larger number than in the two-dimensional case. Here the number of unknown coefficients increases with N^6 as opposed to N^4 for two-dimensional

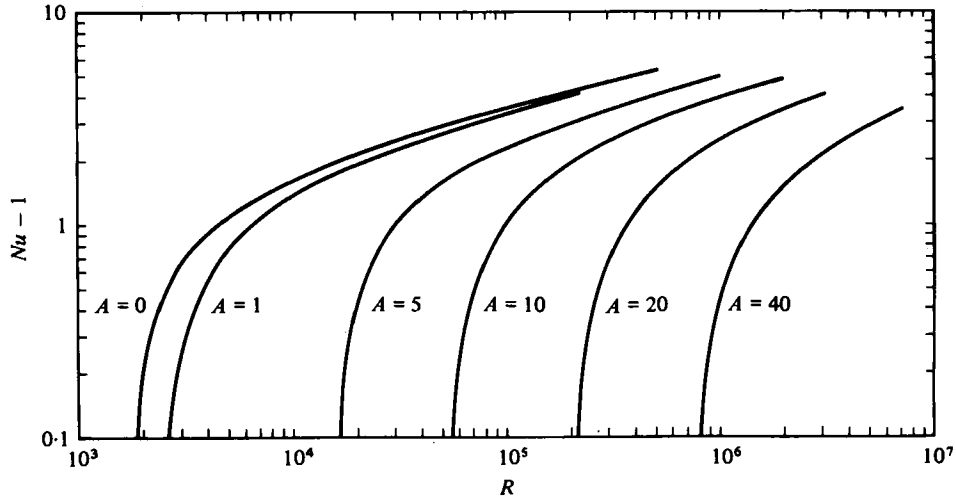

FIGURE 2. The Nusselt number as a function of Rayleigh number for various values of the aspect ratio (given on curves). All curves for $\alpha = \alpha_c$.

convection rolls. Additionally, since the computational cost increases with the number of unknowns to the third power, the addition of the third dimension increases the computational scope enormously. In order to ensure accuracy of the solution we shall increase the value of N, for given fixed values of the parameters R, α and A, until the coefficients with $\lambda+\nu+\beta > N$ contribute negligibly to the solution. This is regarded as satisfactory if the convective heat transport changes by less than 1 % as N is increased to $N+2$ (see Denny & Clever 1974). Representative calculations with larger values of N indicate that this procedure insures accuracy of the solution to within about 1–1·5 % for all values of the parameters investigated.

3. Results

The equations developed in §2 are solved numerically for a wide range of the parameter space R, A and α for various values of the trunction parameter up to $N = 13$. The aspect ratio varies between the limits $0{\cdot}01 \leqslant A \leqslant 100$ in order to approach the limiting cases of a layer of infinite horizontal extent and of Hele Shaw convection. Solutions in the range $R_c < R \leqslant 50R_c$ have been calculated within the limitation imposed by numerical convergence of the solution for sensible values of the truncation parameter. Solutions for various values of the wavenumber, α, have been calculated to determine the influence of wavenumber on the convective heat transport. In order to compare with previous experimental and theoretical measurements of Hele Shaw and porous-medium convection, and expand on several of the assumptions that have been made in previous work, both rigid and stress-free horizontal boundaries have been investigated.

In figure 2 the Rayleigh-number dependence of the Nusselt number for various values of the aspect ratio A at $\alpha = \alpha_c$ is plotted. It is interesting to note the small effect of aspect ratio on the heat transport at large values of the Rayleigh number. For example, at $R = 10^6$ the heat transport across the layer varies by less than a factor of two for aspect ratios in the range $0 \leqslant A \leqslant 20$. For $R = 10^5$ the heat transport at

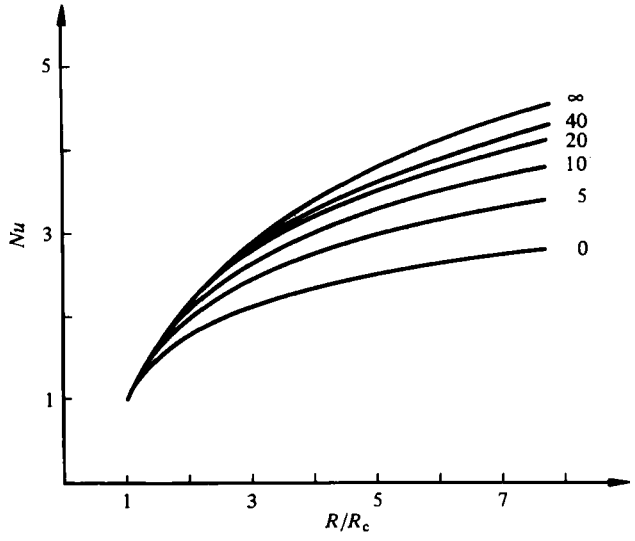

FIGURE 3. Nusselt number as a function of R/R_c for several values of the aspect ratio (given on curves) at $\alpha = \alpha_c$. The results show the strong dependence of Nu on A for large values of A as R/R_c increases from 1.

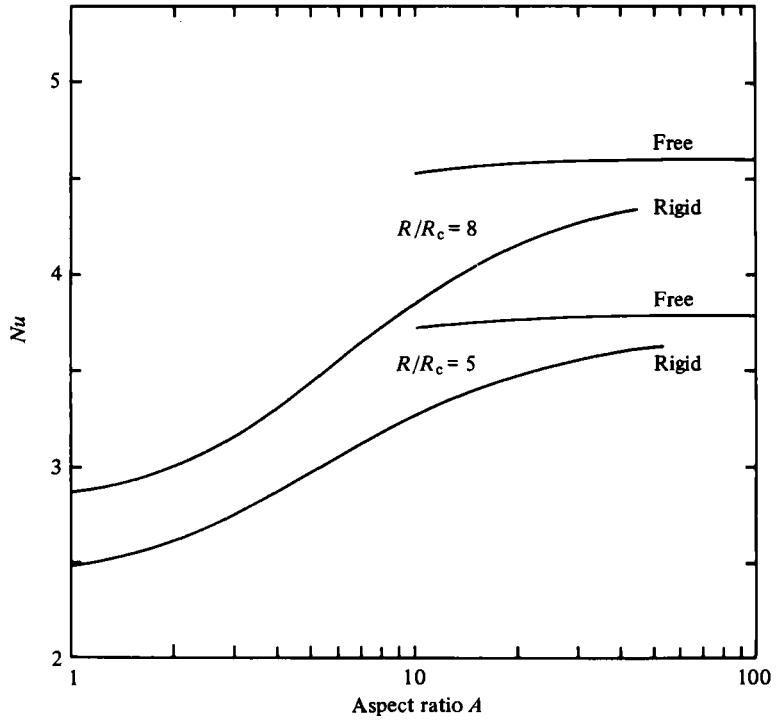

FIGURE 4. Deviation from the Hele Shaw approximation at elevated values of R/R_c for both rigid and stress-free boundaries. Note the more rapid convergence to the asymptotic Hele Shaw results in the case of free boundaries.

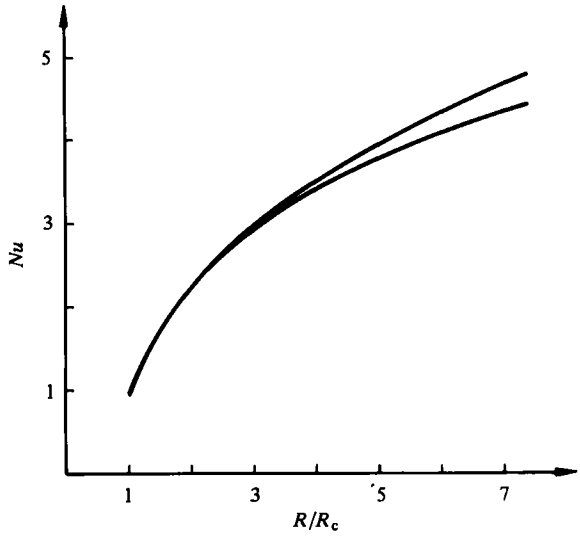

FIGURE 5. The wavenumber dependence of the Nusselt number for convection at $A = 20$ with free boundaries. Lower curve $\alpha = \alpha_c$. Upper curve is calculated with the wavenumber which maximizes the heat transport.

$A = 10$ is already more than a factor of two smaller than for $A = 0$, and for $A = 20$ more than a factor of four. This is caused by both the rather small slope of the Nusselt number $(\partial Nu/\partial R)$ for large-amplitude convection, and the large initial slope for increasing values of A which allows the heat transport to first essentially 'catch up' with the heat transport at small A. We also note that for large values of A the heat transport increases proportionally to $R^{0.3}$, as in the case of two-dimensional Bénard convection. The surprising result that the Nusselt number varies only slightly with the aspect ratio may be contrasted with the asymptotic results for convection in a Hele Shaw cell. Here the Nusselt number and all properties of convection are dependent on the quantity R/A^2 in the limit $A \to \infty$. In the case of small-amplitude convection the Hele Shaw approximation is quite good for $A \gtrsim 20$. At $A = 20$ the critical Rayleigh number agrees to within less than 1%. However, as the amplitude of convection increases, the approximation becomes increasingly less accurate and the value of A required to approach the Hele Shaw results increases strongly with Rayleigh number. In figure 3 the results are plotted using the ratio R/R_c, which is the appropriate scaling parameter for large aspect ratio. As may be seen, the Nusselt number is relatively independent of A for $A \gtrsim 10$ in the neighbourhood of the critical Rayleigh number. However, as the amplitude is increased, deviations from the Hele Shaw approximation occur for all finite values of A. The numerical results indicate that for every value of A the Hele Shaw approximation becomes unsatisfactory for a sufficiently large value of R/R_c. Difficulties in numerical convergence of the solution for very large values of A have precluded quantification of this result.

In order to assess more easily the influence of aspect ratio on the Hele Shaw approximation, the cases of stress-free horizontal boundaries at $R/R_c = 5$ and 8 are compared (figure 4). For both Rayleigh numbers the free-boundary results at $A = 100$ approach reasonably closely the asymptotic Hele Shaw results. On the other hand, the deviation

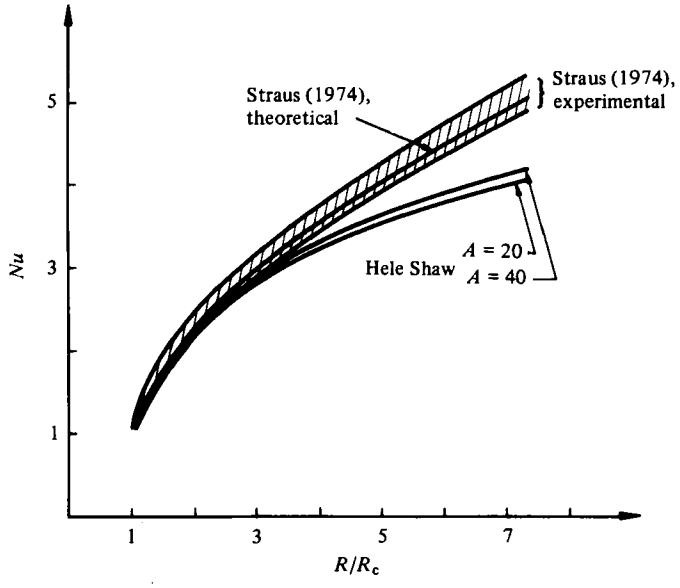

FIGURE 6. Comparison of heat transfer in a Hele Shaw cell and in a porous medium. The shaded area represents the range of experimental values given in Straus (1974). The solid curves for Hele Shaw and porous-medium convection are theoretical calculations.

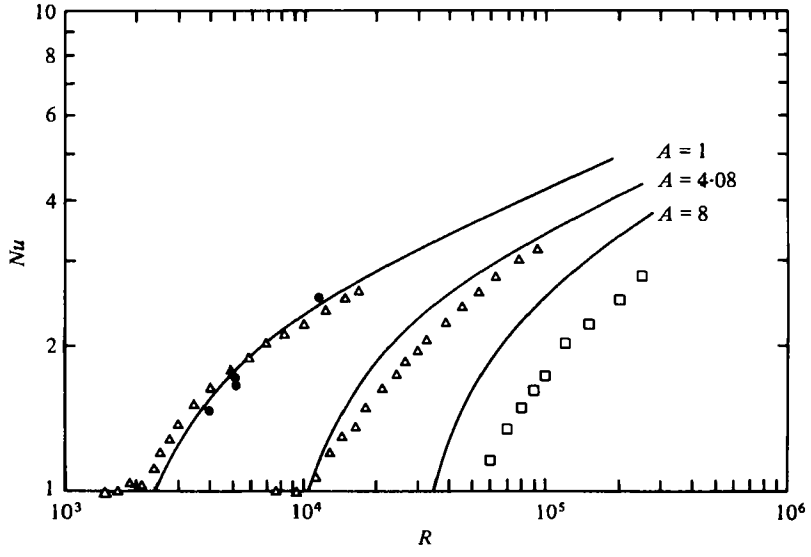

FIGURE 7. Comparison of calculated and measured heat-transfer values for various values of A. Experimental data: △, Arnold (1978); ●, Ozoe *et al.* (1974); □, Wu & Edwards (1980). The present calculations are given by the curves.

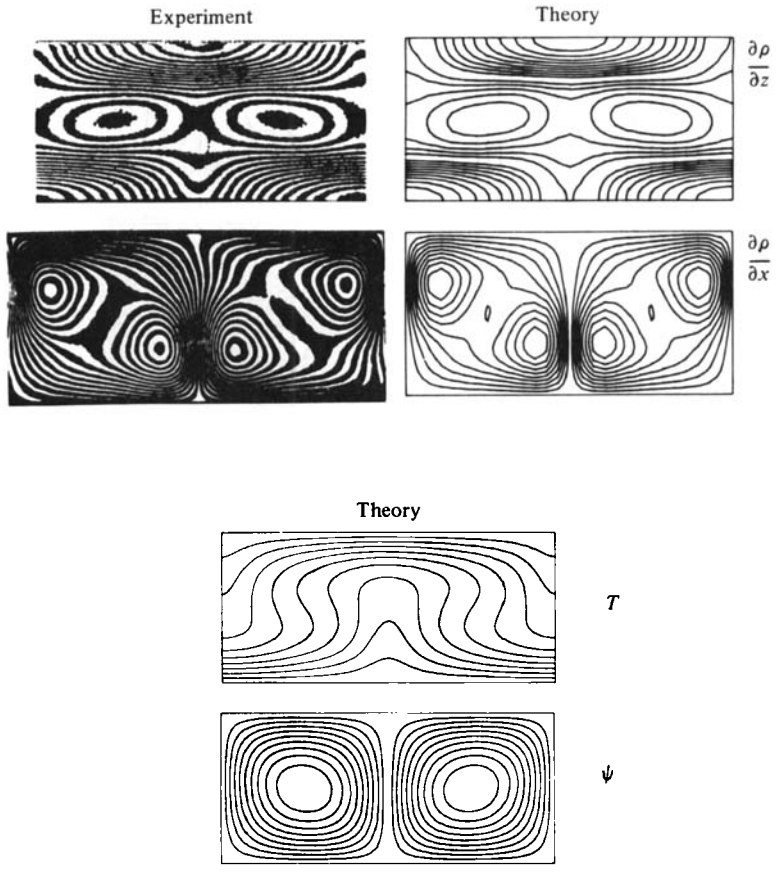

FIGURE 8. Comparison of the temperature and velocity field with the experiments of Bühler *et al.* (1979). $R = 6270$, $A = 0{\cdot}25$.

from the Hele Shaw approximation for finite-amplitude convection in the case of rigid boundaries is clearly noticeable. For $A = 20$ the deviation is already greater than 20 %.

In the limit $A \to \infty$ we obtain an analogy between Hele Shaw convection and convection in a porous medium. In the case of the onset of convection this analogy is exact because the onset of convection in both cases is governed by two-dimensional disturbances. However, for supercritical convection amplitudes there are a number of factors influencing the convection which invalidate this analogy. In addition to the influence of finite aspect ratio for purely two-dimensional convection as discussed above, there seems to be a tendency for the convection wavelength to decrease in the case of porous-medium convection, whereas this mechanism is absent in Hele Shaw convection. Straus (1974) has compared two-dimensional calculations of porous-medium convection with experimental measurements and has found that the heat transport calculated with the wavenumber that maximizes the heat transport gives the best agreement. The results shown in figure 5 indicate the magnitude of this wavenumber effect for two-dimensional convection rolls. Additionally, Straus has shown that above a second critical Rayleigh number two-dimensional convection in a porous medium is unstable to three-dimensional disturbances. In a later paper (Straus & Schubert 1979) three-dimensional convection in a porous medium has been

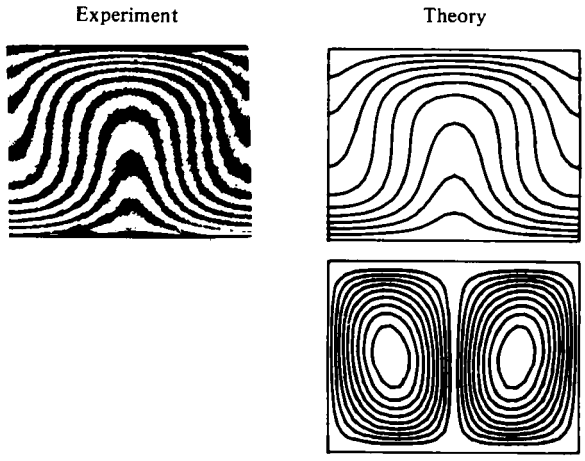

FIGURE 9. Comparison of the temperature field with experimental measurements by Koster (1980) for convection in a Hele Shaw cell. $R = 2R_c$, $A = 18{\cdot}10$, $\alpha = 4{\cdot}8$ (corresponding to the experimental conditions).

considered, and it has been shown that the heat transport is larger than for two-dimensional convection for Rayleigh numbers above 2 or 3 times the critical linear-stability value.

Since each of these effects taken separately serves to increase the heat transport in porous-medium as compared to Hele Shaw convection, increasingly larger heat transport differences between the two cases are expected as the Rayleigh number is increased. In figure 6 we compare previous porous-media results with the heat transport calculated in the present study. It can indeed be seen that large differences occur at large Rayleigh numbers. If the Rayleigh number is increased beyond $R/R_c = 9$, the convection will become time-dependent for the case $\alpha = \pi$ (Kvernvold 1979). Schubert & Straus (1979) obtained non-steady heat-transport fluctuations of two-dimensional convection through porous media for the oscillatory case. The results of Caltagirone (1975) also show that the time-dependent solutions are different from that of the steady solution at a given Rayleigh number. A comparison of the heat-transport results of the present investigation with previous experimental results is given in figure 7. It is worthwhile to note that, at least for $A = 4$, the differences between theory and experiment are approximately as large as the scatter in experimental data. We note also the good quantitative agreement for aspect ratio unity. At $A = 1$, based on the approximation of convection rolls with two velocity components, the largest discrepancy in the calculated values should be expected, and we may conclude that the approximation is justified by the good agreement. For $A = 4$ and especially for $A = 8$ the differences between the present and the experimental results are larger. These differences are caused by deviations from adiabatic side-wall conditions in the experiment, whose effect on Nusselt number increases with increasing aspect ratio.

In addition to the heat transport, which is an averaged property of the convection, it is also of interest to compare more detailed properties of the convection. The streamlines and isotherms for the experimental conditions measured by Bühler, Kirchartz & Oertel (1979) are given in figure 8. In addition figure 8 shows the quantities $\partial\rho/\partial z$ and $\partial\rho/\partial x$ which have been measured by these authors in convection experiments. In principle, one can construct the temperature field from these interferometric

photos, although this has not been done by Bühler *et al.* However, the good agreement in the computation of these quantities allows us to present the temperature fields of these experiments. In figure 9 a comparison with the Hele Shaw experiment of Koster (1980) is presented. Here again we find a good agreement between predictions and measurements. The theoretical predictions shown in figures 8 and 9 are calculated at the $y = 0$ plane.

4. Concluding remarks

In the presence of side walls, strictly two-dimensional convection rolls, depending on all three spatial co-ordinates, must be regarded as an approximation because of the generation of a component of vertical vorticity caused by the temperature gradient parallel to the axis of the rolls. Even in the case of an infinite-Prandtl-number fluid this additional velocity component is required for a general solution. However, nearly all previous investigations have neglected this additional feature in the case of rigid boundaries owing to the added mathematical complexity, even in the solution of the linear problem for the onset of convection. Recent theoretical work on the onset of convection by Davies-Jones (1970), for free boundaries and by Frick & Clever (1980), for rigid boundaries, has demonstrated that the error introduced by this assumption is minor, at least in terms of the value of the critical Rayleigh number. This conclusion is considerably stronger for the rigid-boundary problem. The comparison of the heat transport calculated in the present investigation with experimentally measured values suggests that this assumption remains justified for finite amplitude.

The analogy that exists between Hele Shaw and porous-medium convection in the case of the onset of convection has been generally regarded as a basis for extrapolation into the finite-amplitude regime and comparison between the two cases. The postulated analogy has been convenient and useful in practical application because of the difficulties in observing and properly measuring and quantifying the experimental conditions. The results of the present study demonstrate that changes in the wavenumber and the three-dimensionality of porous media convection cause rather strong deviations from even idealized Hele Shaw convection in the limit $A \to \infty$. Additionally, in the realistic case of finite A, the Hele Shaw approximation becomes inaccurate even for large values of A as the convection amplitude increases. Combining these several effects we find rather large differences between the two cases for Rayleigh numbers greater than a few times the critical value for values of the aspect ratio for which a nearly perfect analogy exists at the onset of convection. As the Rayleigh number is increased further, the deviations increase. In the limit of large Rayleigh number the Nusselt number for Hele Shaw convection has been shown to increase approximately as $R^{0.3}$, whereas for porous-medium convection the Nusselt number typically increases faster than $R^{0.5}$.

We thank Professors U. Müller of the Kernforschungszentrum Karlsruhe and F. H. Busse of UCLA for many helpful discussions during the course of this work. This work was supported by the Deutschen Akademischen Austauschdienstes, the Deutschen Forschungsgemeinschaft and the Atmospheric Science Section of the National Science Foundation.

REFERENCES

ARNOLD, I. N. 1978 Heat transfer by natural convection in enclosed rectangular cavities. Dissertation, University of California, Los Angeles.

BÜHLER, K., KIRCHARTZ, K. R. & OERTEL, H. 1979 Steady convection in a horizontal fluid layer. *Acta Mech.* **31**, 135–171.

BUSSE, F. H. 1967 On the stability of two-dimensional convection in a layer heated from below. *J. Math. & Phys.* **46**, 140–150.

BUSSE, F. H. 1978 Nonlinear properties of thermal convection. *Rep. Prog. Phys.* **41**, 1929–1967.

CALTAGIRONE, J. P. 1975 Thermoconvective instabilities in a horizontal porous layer. *J. Fluid Mech.* **72**, 269–287.

CLEVER, R. M. & BUSSE, F. H. 1974 Transition to time-dependent convection. *J. Fluid Mech.* **65**, 625–645.

CHANDRASEKHAR, S. 1961 *Hydrodynamic and Hydromagnetic Stability*. Clarendon Press.

DAVIS, S. H. 1967 Convection in a box: linear theory. *J. Fluid Mech.* **30**, 465–478.

DAVIES-JONES, R. P. 1970 Thermal convection in an infinite channel with no-slip side walls. *J. Fluid Mech.* **44**, 695–704.

DENNY, V. E. & CLEVER, R. M. 1974 Comparisons of Galerkin and finite-difference methods for solving highly nonlinear thermally driven flows. *J. Comp. Phys.* **16**, 271–284.

EDWARDS, D. K., ARNOLD, I. N. & WU, P. S. 1979 Correlations for natural convection through high-L/D rectangular cells. *Trans A.S.M.E.* C, *J. Heat Transfer* **101**, 741–743.

ELDER, J. W. 1967 Steady free convection in a porous medium heated from below. *J. Fluid Mech.* **72**, 29–48.

FRICK, H. & CLEVER, R. M. 1980 Einfluß der Seitenwände auf das Einsetzen der Konvektion in einer horizontalen Flüssigkeitsschicht. *Z. angew. Math. Phys.* **31**, 502–513.

KOSTER, J. N. 1980 Freie Konvektion in vertikalen Spalten. Dissertation, Universität Karlsruhe (Kfk 3066).

KVERNVOLD, O. 1979 On the stability of nonlinear convection in a Hele Shaw cell. *Int. J. Heat Mass Transfer* **22**, 395–400.

OZOE, H., SAYAMA, H. & CHURCHILL, S. W. 1974 Natural convection in an inclined square channel. *Int. J. Heat Mass Transfer* **17**, 401–406.

SCHUBERT, G. & STRAUS, J. M. 1979 Three-dimensional and multicellular steady and unsteady convection in fluid-saturated porous media at high Rayleigh numbers. *J. Fluid Mech.* **94**, 25–33.

STRAUS, J. M. 1974 Large-amplitude convection in a porous medium. *J. Fluid Mech.* **64**, 51–63.

STRAUS, J. M. & SCHUBERT, G. 1979 Three-dimensional convection in a cubic box of fluid-saturated porous material. *J. Fluid Mech.* **91**, 155–165.

WU, P. S. & EDWARDS, D. K. 1980 Effect of combined tilt and end clearance upon natural convection in high-L/D rectangular honeycomb. *Solar Energy* **25**, 471–473.